



Effects of Injection Pattern Design on Piston Thermal Management in an Opposed-Piston Two-Stroke Engine

2013-01-2423

Published
09/24/2013

Rishikesh Venugopal, Neerav Abani, and Ryan MacKenzie
Achates Power Inc.

Copyright © 2013 SAE International
doi:10.4271/2013-01-2423

ABSTRACT

This paper presents analytical and measured results on the effects of injection pattern design on piston thermal management in an Opposed-Piston, Two-Stroke (OP2S) diesel engine. The OP2S architecture investigated in this work comprises two opposing pistons forming an asymmetric combustion chamber with two opposing injectors mounted on the cylinder wall. This unique configuration offers opportunities to tailor the injection pattern to control the combustion heat flux and resulting temperatures on the piston surfaces while optimizing combustion simultaneously. This study utilizes three-dimensional (3D) computational fluid dynamics (CFD) with state-of-the-art spray, turbulence and combustion models that include detailed chemistry to simulate the in-cylinder combustion and the associated flame/wall interactions. In addition, the measurements comprise a real-time thermocouple system, which allows for up to 14 locations to be monitored and recorded on the intake and exhaust pistons.

The CFD results are shown to predict the measured performance and emissions characteristics with very good correlation. Using the CFD model results, hot spot areas on the piston surfaces—resulting from impingement of the injection plumes during the combustion event—are computed. A proprietary telemetry system using thermocouples at key locations on the piston is deployed to measure the effects of injector clocking and injection spray angle on the piston temperatures. It is demonstrated that the trends in the computed hot spot areas for different injection patterns correlate well with trends in the measured temperatures. Furthermore, the investigations show that the clocking angle

and the spray angle are two critical levers that can be optimized using CFD simulations for piston thermal management in the OP2S configuration. The results of this investigation demonstrate the effectiveness of experimentally correlated combustion-CFD simulations to unlock the potential of the OP2S configuration for improved piston thermal management.

INTRODUCTION

With increasing demand for high-efficiency, emissions-compliant and durable powertrains for transportation and power generation applications, radical advances in reciprocating engine technology are critical. Opposed-piston, two-stroke (OP2S) diesel engines have traditionally provided superior power densities and brake thermal efficiencies as compared to their four-stroke diesel counterparts, but were historically challenged from the standpoint of emissions and durability [1]. More recently, the opposed-piston (OP) concept has received renewed attention, and has been successfully modernized to overcome historical drawbacks and achieve drastic improvements in fuel efficiency relative to state-of-the-art, four-stroke diesel engines [2,3]. OP2S engines have several inherent thermodynamic advantages [4]. These engines eliminate the cylinder head and valvetrain, and comprise two opposed pistons that uncover intake and exhaust ports formed on the cylinder wall. This configuration results in a favorable surface-to-volume ratio, and with the stroke split between the two pistons, relatively large stroke-to-bore ratios can be achieved without excessive mean piston speeds. As discussed by Foster et al. [4], large stroke-to-bore ratios (> 2.0) directly result in improved indicated thermal efficiencies, and facilitate efficient uniflow scavenging during the two-stroke engine cycle. In addition, the two-

stroke operation leads to leaner in-cylinder conditions, which helps to achieve high power densities without excessive pressure rise rates. Several other advantages of the OP2S are documented in the literature [1,2,3,4], including reduced heat transfer, as the pistons can inherently be maintained at a higher metal temperature than cylinder heads in conventional four-stroke engines.

While the OP2S architecture offers numerous advantages and presents a unique configuration for achieving high power densities and low fuel consumption rates with emissions compliance, effective thermal management of the reciprocating pistons is a key design requirement that must be met and optimized. In an OP2S engine, heat transfer to the pistons is strongly influenced by the power cylinder design, including the injection spray pattern, piston bowl shape and port configuration. The injection spray pattern, in turn, is governed by numerous design features, such as number of holes, hole size (or flow rate), injector clocking (i.e. circumferential rotation of the injector) and the injection spray angle (i.e. angle between the spray plumes and the injector axis). Furthermore, these design features pertaining to the injection pattern may be strongly coupled to the charge motion and piston bowl design, and need to be optimized for piston thermal management while maintaining or improving indicated work and emissions characteristics. Note that in a twin-injector OP2S combustion system, there is a great deal of flexibility in the injector configuration to produce strategies, such as injector staggering and injection rateshaping that could offer combined benefits for piston thermal management, performance and emissions. As shown in this paper, computational fluid dynamics (CFD) modeling correlated with engine experiments has proven to be a powerful tool to perform detailed simulations of the in-cylinder flowfield and combustion, and understand the efficacy of numerous levers related to the design of the injection system and combustion chamber.

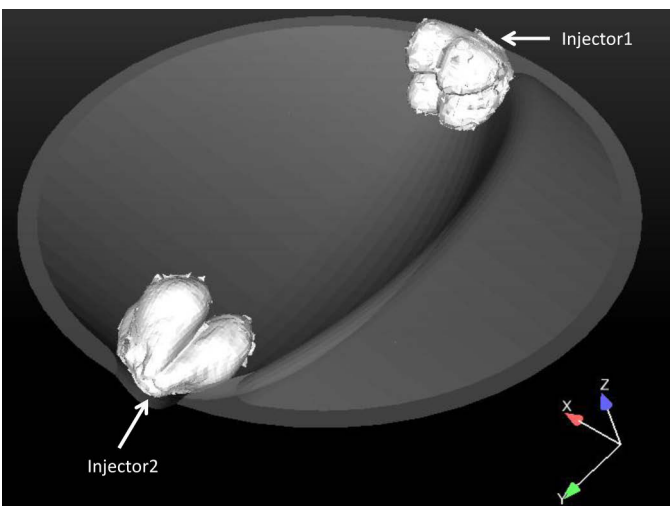


Figure 1. Schematic of the combustion system with two side-mounted injectors

In this paper, the proprietary Achates Power OP2S combustion system [5] with a twin side injector layout is used to investigate the effects of injection pattern design on piston thermal management. Figure 1 shows a schematic of the combustion system with two side-mounted injectors with only the exhaust-side piston shown for clarity. The Achates Power OP2S engine architecture and the demonstrated benefits in terms of fuel efficiency and emissions through extensive dynamometer testing combined with modeling have been documented in several publications [2,3,6,7], and will not be repeated here. This paper will focus on employing a combined experimental and numerical approach to understand and demonstrate injection pattern effects on improving piston thermal management in an OP2S engine. It is noteworthy that the present contribution is unique as piston thermal management studies correlating combustion-CFD simulations to engine experiments are limited in the literature.

ENGINE EXPERIMENTS

The engine experiments described here are performed on a custom single-cylinder research engine manufactured in-house at Achates Power. The engine as shown in Figure 2 has a bore of 98.4 mm, and a stroke of 215.9 mm, resulting in a displaced volume of 1.64 L. The liner geometry creates fixed port timing, and the piston geometry and injection spray pattern have been specified based on combustion simulations. The common-rail fuel injection system is capable of injection pressures up to 2200 bar and can produce multiple injection events per engine cycle.

The conditioned combustion air and EGR are delivered to the intake manifold of the single-cylinder test engine via the system shown in Figure 3. Note that this is a test system setup to simulate a real-world air-handling system. An external air compressor feeds compressed air to the conditioning unit where it is mixed with exhaust gas taken from the exhaust side of the engine. An EGR pump is used to drive exhaust flow through a gas-to-water heat exchanger before delivering exhaust gas to the intake stream. The EGR rate delivered to the engine is controlled by the EGR pump speed and a ball valve located downstream of the pump. After the air and exhaust gas are mixed, the intake gas flows through a second heat exchanger followed by a heater to precisely control the intake manifold temperature. The exhaust manifold pressure is set with a back pressure valve in the exhaust system. The back pressure valve helps establish the pressure difference required to achieve the desired charge flow through the engine. Note that the dataset reported in this study does not incorporate EGR.

In-cylinder pressure is measured at 0.5° crank-angle intervals with a piezoelectric pressure transducer coupled to a charge amplifier. The cylinder pressure signal is pegged to an average of the intake and exhaust manifold pressures during scavenging. These pressures are measured with high-speed pressure transducers, which are capable of measuring absolute pressures. Custom in-house software is used to

acquire and process the data. A California Analytical Instruments (CAI) emissions analyzer is used to measure the steady-state concentration of five exhaust species (CO₂, CO, O₂, HC, NO_x) and intake CO₂. An AVL 415s Smoke Meter provides a measure of exhaust soot content.



Figure 2. Test cell setup of the single-cylinder research engine.

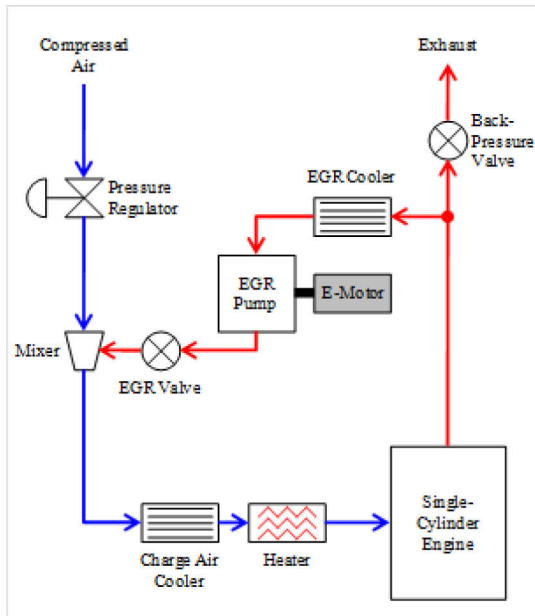


Figure 3. Schematic of the air and EGR conditioning system in the test cell.

A proprietary telemetry system developed in-house is employed to measure temperatures at various locations on the piston. Up to seven locations are monitored per piston in real time, allowing for the study of multiple variables that affect piston temperature. Changes in injector orientation can quickly be evaluated and adjusted to give the optimal temperature profile for combustion, heat transfer and piston durability. The thermocouples are mounted in strategic

locations on the piston bowl, such as the bowl rim, injector trench and top ring land. The remote telemetry is achieved by radio frequency (RF). In a signal conditioning module mounted on the piston, thermocouple (TC) signals are offset by “cold junction” voltage from a sensor and gained up to 0 to 3.0 volts. Amplified and corrected TC signals along with a reference voltage are then time multiplexed and sent to a voltage to frequency (V to F) converter. Converter output modulates the transmitter. At the receiver the demodulated signal is sent to a frequency to voltage (F to V) converter. F to V output is de-multiplexed by a micro controller which also checks the system for proper signal timing. Overall system gain is set using the reference voltage from the signal conditioning module. Individual temperature signals are switched to sample and hold circuits which then relay the signals to the test cell data acquisition system for display and recording. Power is supplied to the piston mounted components of the system by inductive coupling within ± 6 degrees centigrade (C) from bottom dead center. The data acquisition rate is one data point per second, and the measurements are accurate within ± 3 degrees C.

The thermocouples measure the temperature approximately 2 mm below the combustion surface. A thermal finite element analysis (FEA) with temperature dependent material properties is used to extrapolate to the surface to get a cycle-averaged surface temperature. This surface temperature must remain below a set limit of 520 degrees C to avoid oxidation and fatigue failure due to compromised material properties at the combustion chamber surface. On the under crown, this temperature must not exceed 285 degrees C to avoid oil coking. The FEA model is validated by comparing against the thermocouple measurements at various locations on the piston. The description of the FEA model and results is outside the scope of this work, but the trends from the thermocouple measurements for different injection patterns are directly compared with predictions from the combustion-CFD model described in the subsequent sections. It is shown that the combustion-CFD results consistently predict the measured trends with respect to injection pattern variation, and help identify the favorable hardware combinations and the governing mechanisms for improved piston thermal management.

Engine Operating Conditions

Table 1. Details of the 50% load operating condition

Speed	2400 RPM
IMEP	7.7 bar
Total fuel mass	56.7 mg
Start of injection	-6.0 degree aMV
Injection duration	11.4 degree
Injection pressure	1200 bar
Trapped A/F	51.6

Table 2. Details of the 70 % load operating condition

Speed	2400 RPM
IMEP	12.1 bar
Total fuel mass	96.0 mg
Start of injection	-2.0 degree aMV
Injection duration	18.6 degree
Injection pressure	2000 bar
Trapped A/F	34.4

Tables 1 and 2 summarize the operating conditions investigated in this study. Note that these operating conditions correspond to 50% and 70% load, respectively, on the single-cylinder engine, where tradeoffs between performance and piston thermal management are important. Under these conditions, higher indicated thermal efficiency resulting from shorter burn duration and higher in-cylinder peak temperature could increase local hot spots on the pistons (arising from flame-wall interactions) and resulting piston temperatures. It is therefore important to understand the tradeoffs between maintaining good efficiency and acceptable piston thermal management. Also, note that the conditions discussed here do not incorporate EGR, which in turn represent more challenging scenarios for piston thermal management owing to higher in-cylinder temperatures. In Tables 1 and 2, crank angle is reported in degree aMV, where aMV stands for after-minimum-volume, where minimum volume is the smallest volume reached between the two opposing pistons during the closed cycle.

COMBUSTION-CFD MODEL CORRELATION

In this section, correlation of the combustion-CFD model employed in this study with measured data is presented for the conditions reported in Tables 1 and 2.

CFD Model Description

A modified version of the commercially available CONVERGE CFD software [8, 9] is used to perform in-cylinder simulations of the OP2S combustion system. The modifications to the standard version of CONVERGE include user defined functions for simulating opposing piston motions, and computation of several performance, emissions and thermal management metrics. Figure 4 shows the triangulated surface description of the closed-combustion model with intake and exhaust pistons at their maximum separation. Intake and exhaust port geometries are not included as only the closed portion of the cycle from exhaust port closing (= -122 degree aMV) to exhaust port opening (=110 degree aMV) is simulated. The initial flowfield is derived from an open cycle CONVERGE simulation that simulates the gas exchange process from intake port opening to exhaust port closing. The trapped pressure is specified based on the cylinder pressure measurements, and the trapped composition and temperature are obtained from a well-correlated (to single cylinder engine measurements) one-dimensional GT-Power model predictions. Note that

CONVERGE generates a volume mesh automatically at every time step. Both adaptive mesh refinement and fixed grid embedding techniques [9] are employed to sufficiently resolve gradients in the flowfield and essential flow features. Grid sensitivity studies showed a resolution in the range of 0.5-2.0 mm throughout the domain provided adequate qualitative and quantitative agreement with measured data, and the best compromise between runtimes and accuracy. A detailed chemistry model involving a well-known reduced chemistry mechanism for n-heptane (diesel fuel surrogate) with 35 species and 77 reaction steps [10], which include a NOx submechanism, is used. Soot emissions are modeled using a two-step model, which includes a Hiroyasu formation step with acetylene as the precursor [11], and an oxidation step involving carbon oxidation by O2 molecules [12]. Sprays are modeled using a modified KH-RT breakup model without the use of an ad-hoc breakup length [9, 13] and the O'Rourke collision model [9, 14], whereas turbulence is modeled using the RNG k-ε model [9, 15]. Fuel injection rate profiles are specified based on measured data from a state-of-the-art, in-house fuel laboratory with IFR (Injection Flow and Rate) capabilities [16].

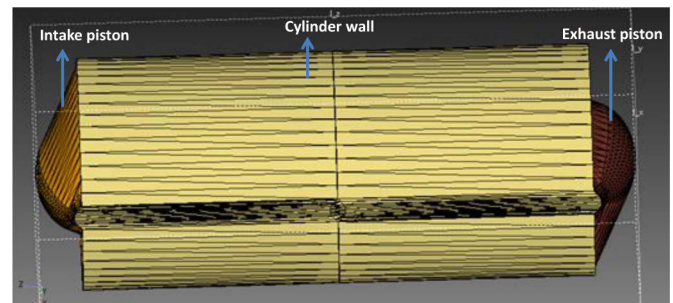


Figure 4. Triangulated surface description of the closed volume geometry used in the CFD simulations.

Model Correlation at 50% Load

Figure 5 shows the comparison of the measured cylinder pressure trace and the predicted pressure from the CFD simulation. The peak cylinder pressure is overpredicted by about 2.5% relative to the measured trace, but overall good agreement is obtained with the measured data. Also compared in Figure 5 are the heat release rates calculated from both the measured and simulated pressure traces. The model predictions show very good agreement in terms of the shape of the heat release profile. To further quantify the comparison of the pressure traces between measured and simulated results, consider Figure 6, which summarizes the 10-90 burn duration (CA10-90), and the closed cycle power (CCP) in KW computed using the expression:

$$CCP = \left(\int_{EPC}^{EPO} P dV \right) * RPM / 60,000 \quad (1)$$

where EPO and EPC are the exhaust port opening and closing crank angles, respectively, P is the cylinder pressure and V is the chamber volume at a given crank angle, and RPM is the engine speed in revolutions per minute. Here, CA10-90 is the burn duration computed as the difference between CA90 and

CA10, which are the crank angles at which 90% and 10% of the total cumulative heat release are reached. As seen from Figure 6, the 10-90 burn duration predicted by the model agrees within 5.5%, whereas the closed-cycle power agrees within 4%. Note that the present modeling approach employs a uniform piston wall temperature assumption, which may not be fully adequate to predict heat transfer to the walls, and hence CCP with better accuracy. While more complex approaches, such as conjugate heat transfer, can help improve heat transfer and CCP predictive capability, the simpler uniform wall temperature approach was chosen for this study as the best compromise between feasible computational times and accuracy. Also shown in Figure 6 are the predicted NOx and soot emissions normalized by the measured value. Very good agreement is seen for NOx emissions, and the agreement in terms of soot emissions is encouraging as well given that the fuel-specific soot emissions measured at this condition is about 0.1 g per kg of fuel.

Figures 7 and 8 show the comparison of measured and simulated results at the 70% load operating condition. Note that the model employed at this operating condition is identical to that at 50% load in terms of the turbulence and spray model parameters. Very good agreement is obtained between the measured and simulated results in terms of the 10-90 burn duration, while CCP agrees within 3.5%. With respect to emissions, NOx predictions agree within 5%, while soot emissions are under-estimated. Overall, the employed combustion modeling framework captures the combustion characteristics well for both the operating conditions investigated in this study.

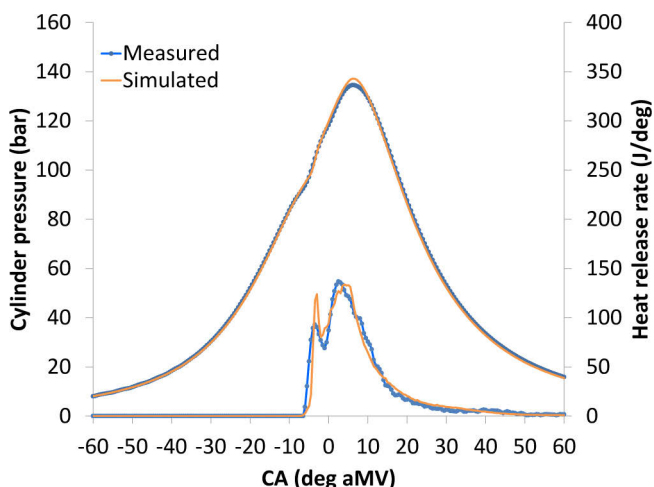


Figure 5. Comparison of measured and predicted pressure trace and the corresponding heat release rates at 50% load.

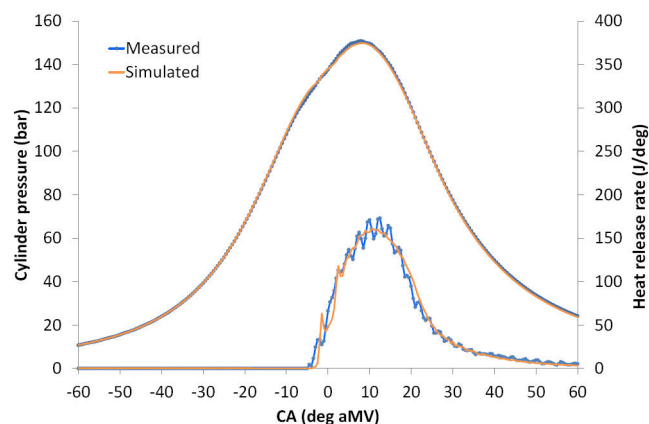


Figure 7. Comparison of measured and predicted pressure trace and corresponding heat release rates at 70% load.

Model Correlation at 70% Load

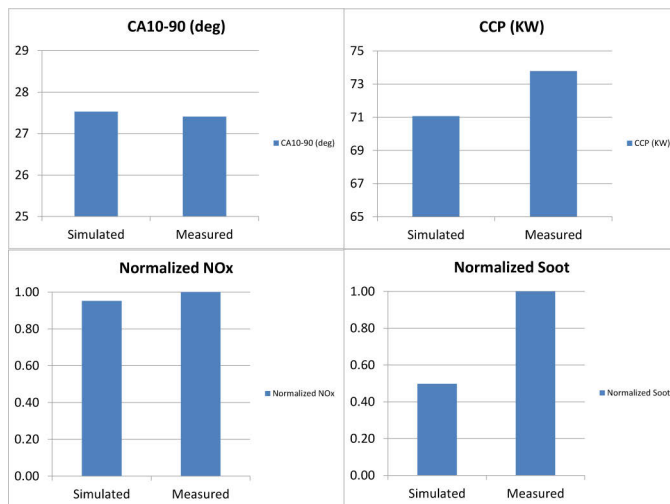


Figure 8. Comparison of measured and predicted performance and emissions at 70% load.

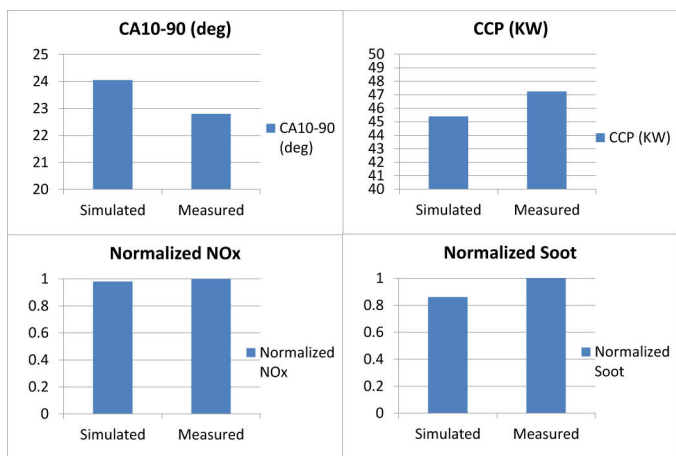


Figure 6. Comparison of measured and predicted performance and emissions at 50% load.

Injection Pattern Effects on Piston Thermal Management

In this section, measured and CFD results are presented, which demonstrate the effects of injection pattern design on piston thermal management. Here, injection pattern design is characterized by the injector clocking angle and the injection spray angle. In the next subsection, the effects of the injector

clocking angle are discussed, and thereafter results pertaining to spray angle variation are presented.

Injector Clocking Effects

Figure 9 depicts the different injector clocking arrangements investigated with the 4-hole injector employed in this study. In Figure 9, the arrows represent individual spray directions projected on a plane in the 4-hole injection pattern. As an example, only Injector 2 is shown with respect to the exhaust-side piston in Figure 9, but similar clocking arrangements can be implemented on Injector 1 as well. Note that while A represents no clocking, B and C represent positive clocking by different amounts, whereas D represents a negative clocking angle. Note that the clocking angle measured about the reference axis shown in the figure in the counterclockwise sense is smaller for the B arrangement relative to the C arrangement. As seen from the figure, the clocking arrangement can strongly influence the impingement of the plumes locally on the bowl lip surface during the injection and combustion events, and hence the resulting piston temperatures. In this section, test and CFD results are presented for three different clocking arrangements at the 50% load condition, Clocking 1: B-A, Clocking 2: B-B, and Clocking 3: D-D, where B-A stands for clocking angle B on Injector 1 (see Figure 1 for injector reference), and clocking angle A on Injector 2, and likewise for the clocking arrangements 2 and 3. Note that the model correlation results shown in the previous section for the 50% load condition corresponds to the Clocking 1 arrangement (B-A).

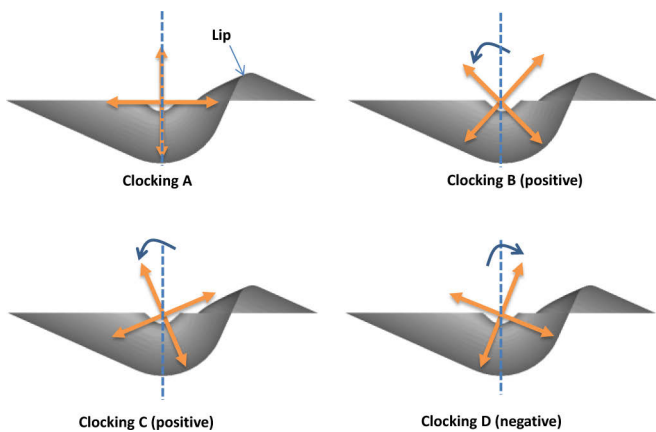


Figure 9. Clocking arrangements investigated for the 4-hole injector

Predicted and measured cylinder pressure and heat release rate are compared for Clocking 2 (B-B) and 3 (D-D) arrangements in Figures 10 and 11, respectively, at the 50% load operating condition. Note that the model is employed with identical spray and turbulence parameters as for Clocking 1, and it predicts the combustion behavior at the other two clocking arrangements reasonably well. For conciseness, the detailed performance and emissions comparisons are skipped, but it is noteworthy to mention that injector clocking has moderate effects on CCP (within $\pm 1\%$) and emissions for the conditions investigated here.

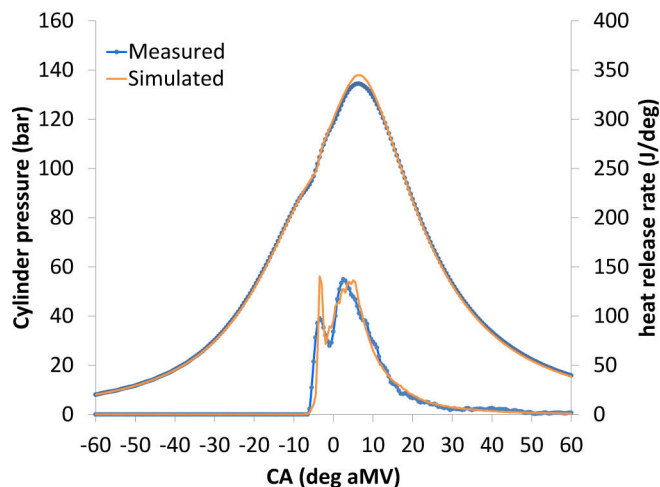


Figure 10. Comparison of measured and predicted cylinder pressure and heat release rate for Clocking 2 arrangement.

Figure 12 shows the piston surface and a cut section to illustrate the location of the thermocouples used for the piston temperature measurements. Note that for the tests reported here, six thermocouples were employed. It is observed in Figure 12 that three thermocouples (1, 5 and 6) are used to characterize the piston lip temperature. These thermocouples are located approximately 2 mm below the piston bowl surface. Measurements showed that locations 1, 5 and 6 on the bowl lip recorded the highest temperatures, and hence the comparison with measured temperatures is focused on the lip region indicated on Figure 12. As will be discussed later, it is shown that the lip surface is exposed to hot gases from the impinging diffusion plumes soon after ignition, which significantly influences heat transfer and resulting piston temperatures. On the other hand, keeping the plumes away from the piston crown surface is very beneficial in limiting heat flow as air is an excellent insulator.

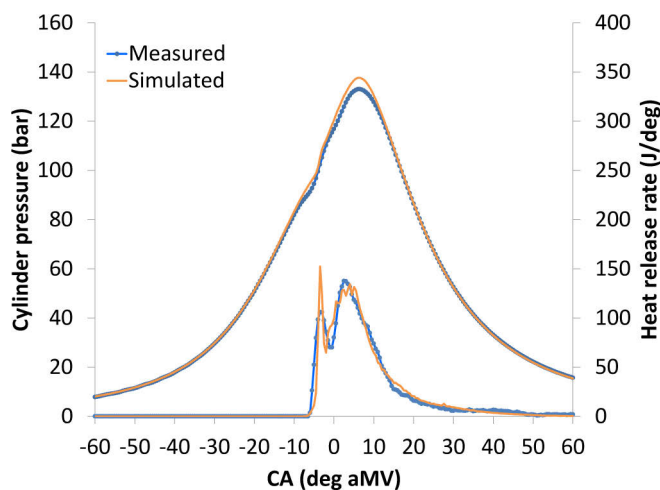


Figure 11. Comparison of measured and predicted cylinder pressure and heat release rate for Clocking 3 arrangement.

It is interesting to observe the trends in the average measured temperatures on the bowl lip (i.e. average of temperatures in 1, 5 and 6 locations) in [Figure 13](#) for different clocking arrangements. Since the primary focus is on understanding trends, [Figure 13](#) reports the intake and exhaust piston lip temperatures as differences (i.e. changes in temperature) with respect to a Baseline, which corresponds to the exhaust lip temperature for Clocking 1 (B-A) arrangement. Note that the lip temperature is computed as the average of measurements at locations 1, 5 and 6. Note that the temperatures reported are cycle-averaged as crank-resolved information cannot be obtained from thermocouples. From the figure, it is clear that both Clocking 2 (B-A) and Clocking 3 (D-D) arrangements result in lower piston lip temperatures, with Clocking 3 yielding more than 8 degree C reduction on the exhaust-side. In addition, the measurements indicate that the intake piston is significantly cooler than the exhaust piston. This is expected as the intake-side is exposed to cooler intake charge during the scavenging process.

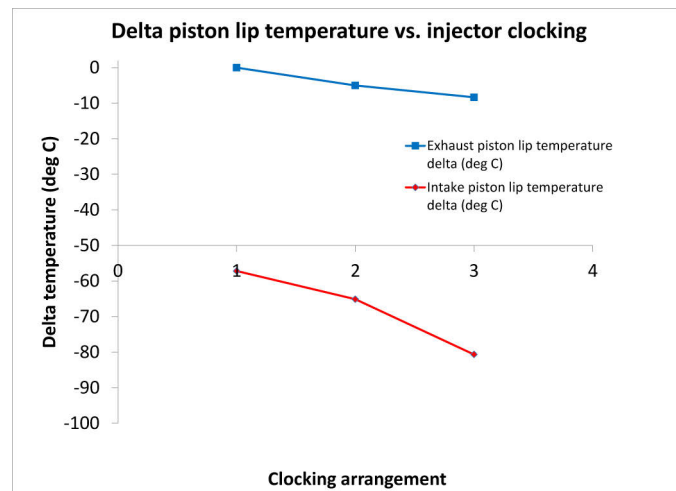


Figure 13. Measured change in temperature with respect to Baseline for Clocking 1 (B-A), Clocking 2 (B-B) and Clocking 3 (D-D) arrangements.

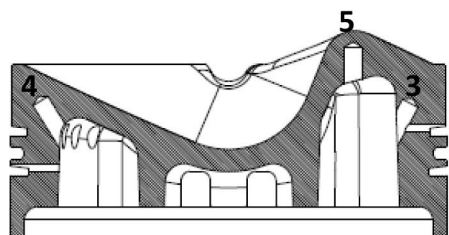
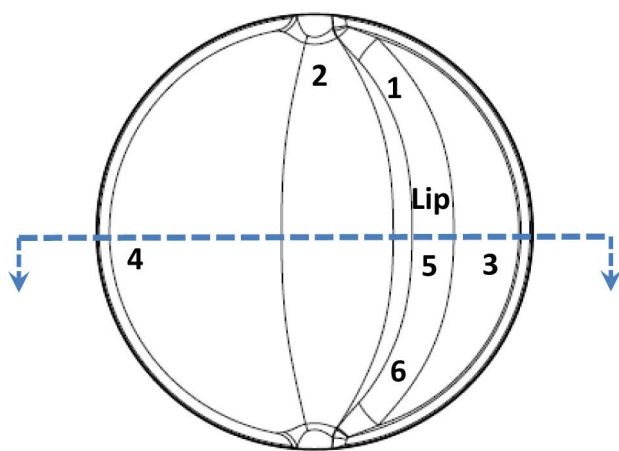


Figure 12. Piston surface and cut section showing thermocouple locations.

Note that these measured thermocouple temperatures are not directly used in the CFD simulations to provide boundary conditions on the piston surface. Instead, these measurements are used in a qualitative sense to identify the problem areas (such as the lip) on the piston surface with respect to thermal management. Moreover, in the next section, the predicted trends from CFD are directly compared with the trends from the thermocouple measurements to improve the understanding of the measured results, and to demonstrate a predictive process for identifying the optimum injection pattern for improving piston thermal management.

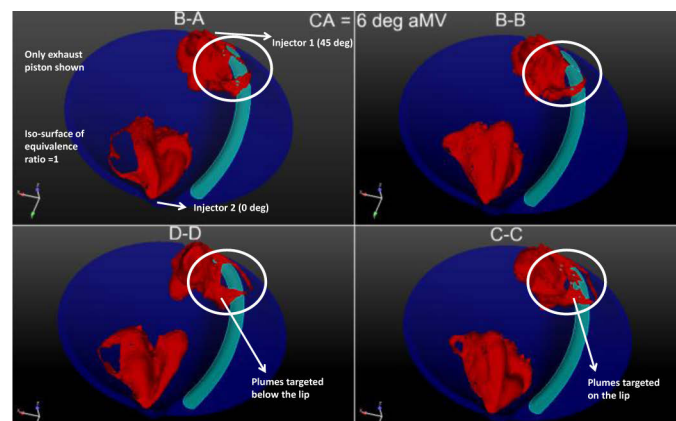


Figure 14. Plume/wall interactions for different clocking patterns at 6 degree aMV crank angle.

Consider [Figure 14](#), which depicts the plume/wall interactions for the four different clocking patterns at 6 degree aMV. Note that though measured data was not collected for the C-C arrangement, CFD results are shown for completeness, and this scenario is referred to as Clocking 4. In this figure, the iso-surface of the stoichiometric mixture (i.e. equivalence ratio of 1) is plotted, and only the exhaust piston is shown for clarity. It is evident from [Figure 14](#) that the clocking pattern on Injector1 influences the impingement and subsequent spreading of the diffusion plumes on the bowl lip surface. It is seen that Clocking 3 (D-D) results in impingement of the plumes below the lip surface, which would reduce the surface area of the lip exposed to the hot gases. On the other hand, Clocking 4 (C-C) results in direct impingement on the lip, and significant spreading of the hot gases on the lip surface are observed. This is evident from [Figure 15](#), which shows the piston surface colored by the near-wall gas temperature. In other words, [Figure 15](#) directly correlates the plume/wall interactions seen in [Figure 14](#) with the resulting hot spots on the piston. Also, note that due to the relatively high swirl employed here, as well as due to a relatively lower power operating condition (50% load), the

plumes from the two injectors do not directly interact in the center of the combustion chamber. This behavior is contrasted from that at the higher power condition explored in the next subsection.

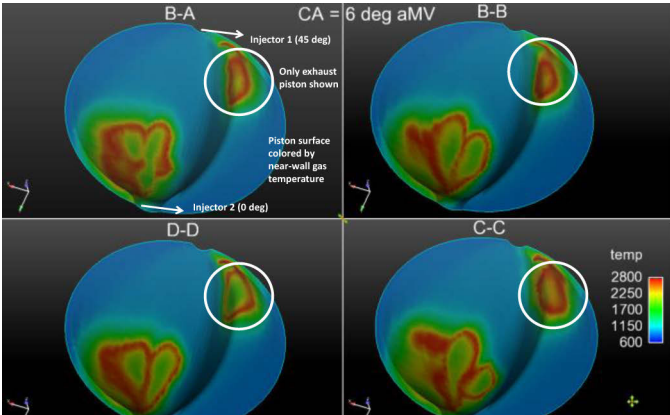


Figure 15. Near-wall gas temperature (in K) on the exhaust piston surface for different clocking patterns at 6 degree aMV crank angle.

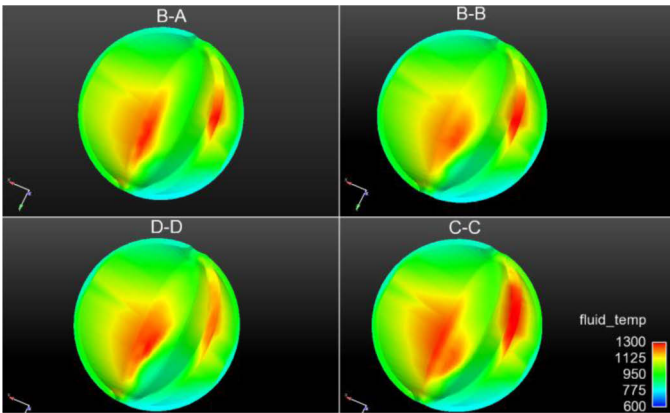


Figure 16. Exhaust piston bowl surface colored by cycle-averaged near-wall gas temperature (in K).

It is noted that while Injector 1 plumes are shown to impact the exhaust piston lip in Figure 14, Injector 2 is more relevant for hot spots on the lip of the intake piston. This behavior is primarily due to the preferential direction of swirl, which acts to deflect Injector 1 plumes towards the exhaust piston lip and the Injector 2 plumes towards the intake piston lip. As discussed earlier (see Figure 13), the intake piston lip is exposed to cooler charge during scavenging, and hence not critical from a thermal management standpoint. Hence, the present analysis focuses on the thermal management of the exhaust piston.

The cycle-averaged near-wall gas temperature is plotted and compared for different clocking arrangements in Figure 16. Differences between Clocking 1 and 2 are more subtle, but similar to the instantaneous results shown in Figure 15, the average temperatures clearly show Clocking 3 as the most favorable arrangement from the standpoint of reducing heat transfer to the piston lip surface, whereas Clocking 4 results in higher gas temperatures near the lip. Though these visual

inspections are indicative of trends, a novel methodology is developed to quantify the transient flame/wall interactions and better correlate trends from measured temperature data.

The instantaneous impingement of the plumes on the piston surface and the strength of the resulting plume/wall interaction are quantified by computing the transient *hot spot area*. The hot spot area is defined as the surface area of the piston exposed to hot combustion gases in a certain temperature range. For instance, consider Figures 17 and 18, which show the computed hot spot areas on the entire exhaust piston (including the bowl lip), and only on the exhaust piston lip region, respectively. It is observed from the figures that the hot spot areas reach a peak at a certain crank angle and thereafter decay during the combustion cycle. Note that the hot spot areas shown in the figures are computed over two temperature bins of equal width designated as “Low” and “High”. Here, these bins are chosen based on the maximum flame temperature attained during the calculation, T_{max} , as follows:

$$0.9T_{max} \leq T_{near\ wall} \leq T_{max} \quad (\text{High}) \quad (2)$$

$$0.8T_{max} \leq T_{near\ wall} < 0.9T_{max} \quad (\text{Low}) \quad (3)$$

In the equations above, $T_{near\ wall}$ is the near-wall gas temperature, and T_{max} is an average of the maximum flame temperatures attained over all the simulations (i.e. Clocking 1-4) considered in this comparison. This way the hot spot areas are computed over identical High and Low temperature bins for all the clocking arrangements. Note that the hot spot areas over the High and Low temperature bins are computed as summations over all the numerical cells that satisfy Equations 2 and 3, respectively. The High and Low bins are chosen to represent the instantaneous interactions of the hot gases (with temperatures higher than 80% of the maximum flame temperature over the cycle) with the piston walls during the injection and combustion events, and the hot spot areas provide a means to quantify these interactions. Though somewhat arbitrary, this choice of temperature bins was tested over a wide range of datasets beyond those considered in this paper, and found to correlate well with measured trends in piston temperatures. These datasets included timing sweeps for injectors with different flow rates for a range of load points.

It is observed from Figures 17 and 18 that the hot spot areas computed on the lip region alone are much smaller in magnitude relative to the entire piston. However, given the relative difficulty of cooling the lip region, it is this region that is most critical for piston thermal management. It is also interesting to note that on the lip region, higher peak hot spot areas from the High bin are observed relative to the Low bin, whereas the trends are reversed when the hot spots are computed on the entire piston. This indicates the lip region is largely exposed to the highest temperature gases soon after ignition and during the early phase of combustion. Now, the trends in the computed hot spot areas are correlated with

trends in the measured bowl lip temperatures for different clocking patterns.

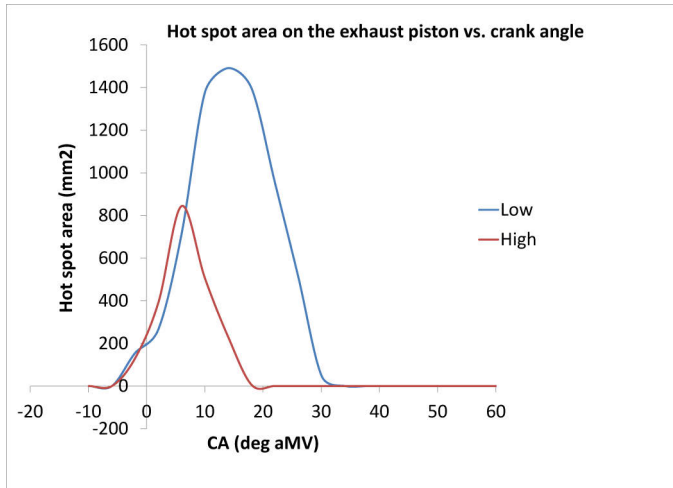


Figure 17. Transient hot spot areas on the exhaust piston as a function of crank angle for the Baseline (Clocking 1) configuration at 50% load conditions.

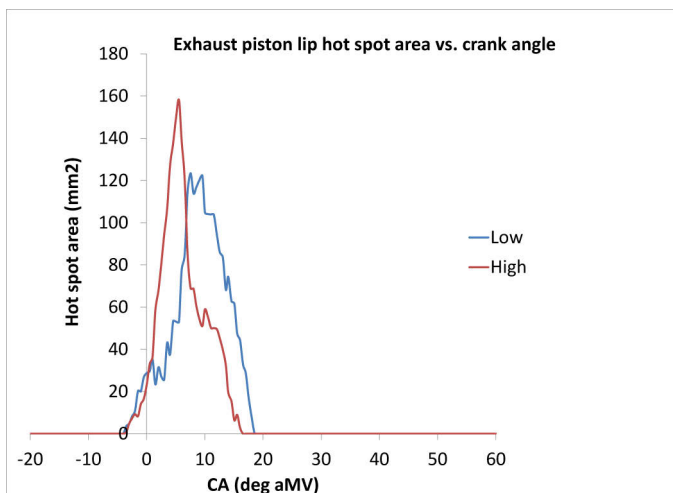


Figure 18. Transient hot spot areas on the exhaust piston lip as a function of crank angle for the Baseline (Clocking 1) configuration at 50% load conditions.

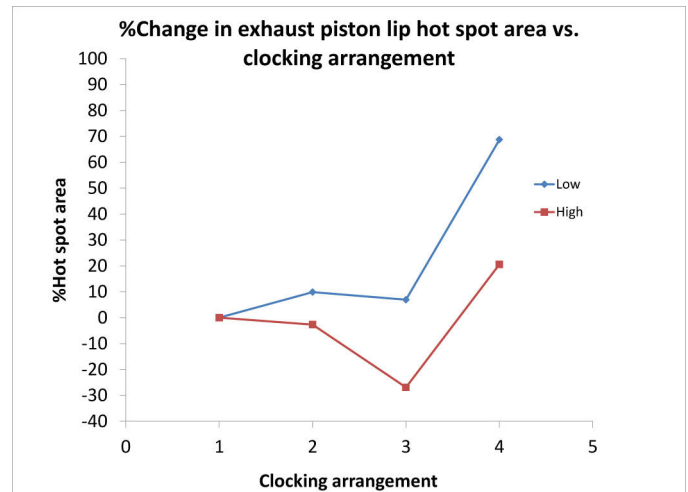


Figure 19. Percentage change (with respect to the Baseline configuration) of average hot spot area on the exhaust piston lip for different clocking arrangements.

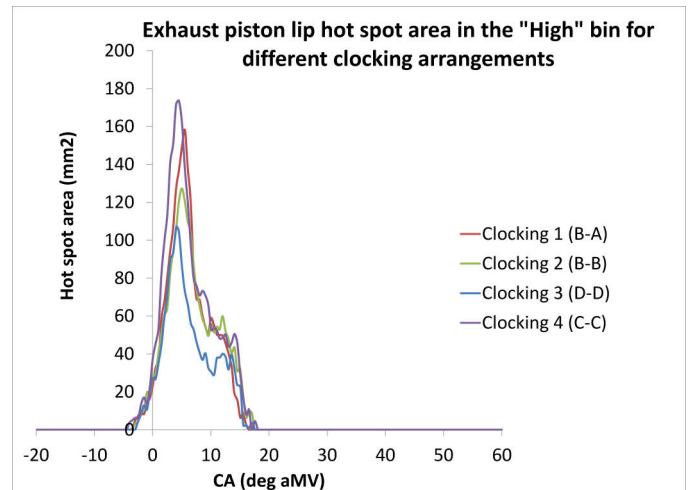


Figure 20. Comparison of computed exhaust piston hot spot areas in the High bin between the different clocking arrangements.

Figure 19 compares the average hot spot area (computed over the closed cycle) on the exhaust piston lip for different clocking arrangements. It is observed that Clocking 3 (D-D) results in a significant reduction in the hot spot area in the High bin relative to the Baseline, whereas the hot spot area in the Low bin shows a moderate increase. In other words, Clocking 3 improves piston thermal management by redistributing the heat input to the piston lip surface from the combustion gases to a lower temperature zone. Similarly, Clocking 2 (B-B) offers a moderate decrease in the High bin hot spot area relative to the Baseline. In good agreement with the images shown in Figures 15 and 16, Clocking 4 (C-C) represents the worst-case scenario for piston thermal management by resulting in a significant increase in the hot spot areas on both the Low and High temperature bins.

These trends are further confirmed through the detailed crank-resolved comparisons of exhaust piston lip hot spot areas in the High and Low temperature bins for the different clocking arrangements in Figures 20 and 21, respectively. It is clearly seen in Figure 20 that the D-D arrangement yields significantly lower peak hot spot area in the High bin, whereas the C-C arrangement yields the highest value during the closed cycle. The differences between the hot spots resulting from the B-A, B-B and D-D arrangements in the Low bin are smaller as seen from Figure 21, but it is expected that the High bin hot spot area has the largest influence on the resulting piston surface temperatures. Figure 22 shows the correlation between the trends in the measured piston lip temperature change (with respect to the Baseline) with the percentage change in the lip hot spot area in the High temperature bin. Note that as in Figure 13, the lip temperature reported in Figure 22 is the average of thermocouple measurements at locations 1, 5 and 6. Trends agree between the measured temperatures and computed hot spot areas, i.e.

Clocking 3 yields the lowest exhaust bowl lip temperatures, and the lowest hot spot area in the High temperature bin. Hence, the combustion-CFD simulations help identify the most favorable clocking arrangement for piston thermal management, and provide insight into effects of clocking in terms of hot spot areas in different temperature bins. It is observed that the sensitivities are different between the measured temperature changes and the percentage changes in hot spot area. This is not surprising, as the hot spot area represents an instantaneous thermal effect on the piston surface, whereas the measured temperature represents steady-state response of the piston over several engine cycles. Accordingly, [Figure 16](#) shows that the trends in the cycle-averaged near-wall gas temperature also agree with the trends in thermocouple measurements. However, the transient hot spot area approach helps understand the underlying mechanisms, such as spray targeting and instantaneous impingement on the bowl lip that govern the effects of injector clocking on piston thermal management.

Spray Angle Effects

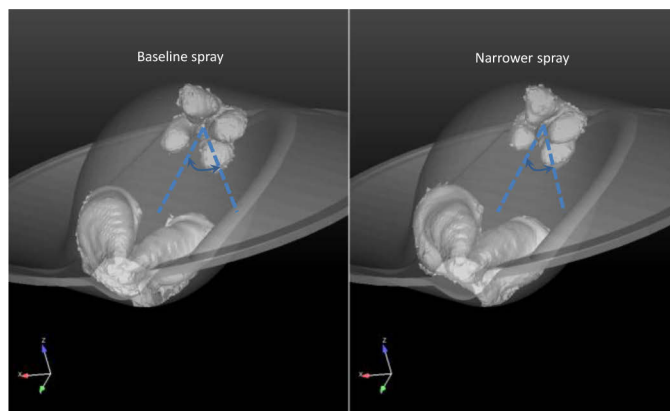


Figure 23. Stoichiometric isosurfaces showing how the spray angle is defined and differences in plume structure between the Baseline and Narrower spray angle scenarios.

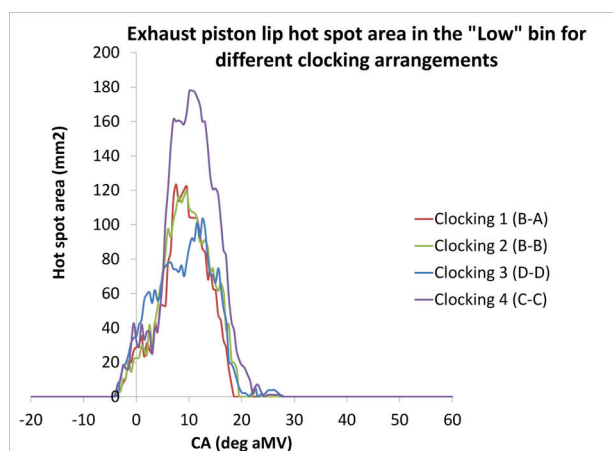


Figure 21. Comparison of computed exhaust piston hot spot areas in the Low bin between the different clocking arrangements.

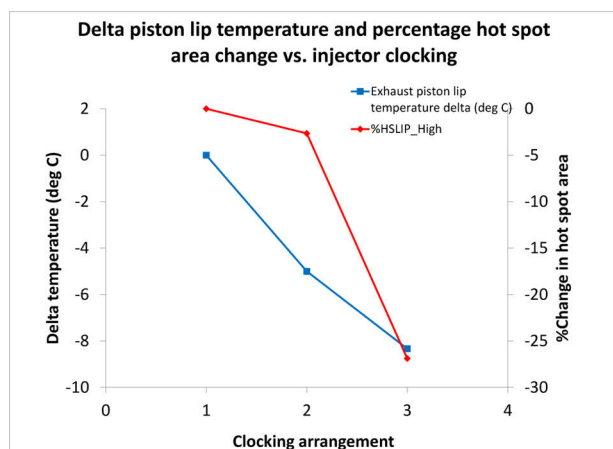


Figure 22. Correlation between measured change in piston lip temperature and percentage change in piston lip hot spot area for different clocking arrangements.

In this section, measured and analytical results for spray angle variation at the 70% load operating condition are discussed. As shown in [Figure 23](#), the spray angle is defined here as the angle between each of the plumes of the 4-hole injector and the injector axis. It is observed in [Figure 23](#) that as the spray angle becomes narrower, the plumes of a given injector are drawn inward more, which under the influence of swirl motion could result in plume-to-plume interactions. In addition, narrower spray angle would limit air entrainment into the spray, but promote combustion more in the center of the chamber and away from the walls. It is therefore important to explore the tradeoffs between performance/emissions and piston thermal management when the spray angle is varied. As in the case of the clocking study, the transient hot spot area method is employed in the simulations to understand and correlate the impact on piston thermal management to measurements. The comparison will be presented between the Baseline spray angle injector discussed in the model correlation section at the 70% load condition, and an injector with a 2.5 degree narrower spray angle. Note that the injector clocking for these tests and simulations was set at Clocking 3 (D-D) to minimize the piston temperatures as revealed from the clocking studies at the 50% load conditions. [Figure 24](#) shows the measured and simulated cylinder pressure and the corresponding heat release rates. Note that the excitation frequencies observed on the measured heat release may be affected from the mounting of the pressure transducer, which are different from the ones due to chemistry-driven autoignition events on the computed heat release. As before, the combustion model is exercised in a predictive mode with identical spray and turbulence model settings as the Baseline model at 50% load. The comparison in [Figure 24](#) reveals good agreement between measurements and predictions. Though the detailed performance and emissions comparisons are skipped here for brevity, it was found that the predicted burn duration for this narrower spray angle scenario agreed within 5%, while the predicted closed-cycle power agreed within 3% of the measured results.

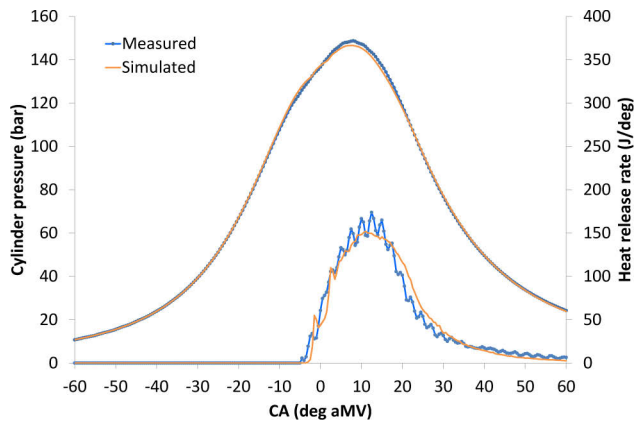


Figure 24. Measured and simulated cylinder pressure and corresponding heat release rates with narrower spray angle injector at 70% load conditions.

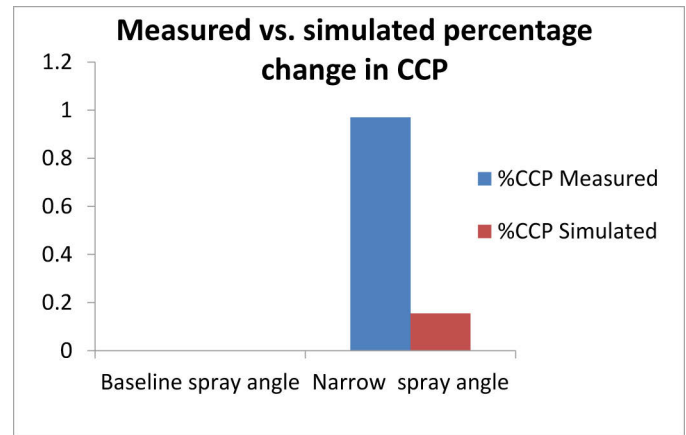


Figure 26. Comparison of the percentage change in CCP based on measured and simulated results for spray angle variation at 70% load.

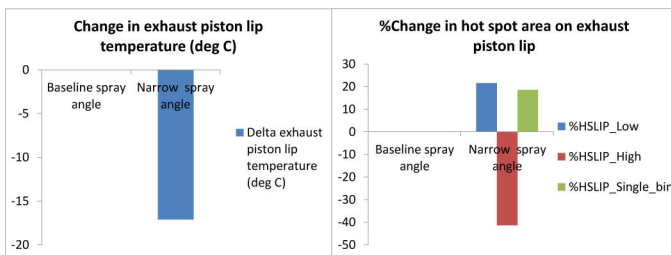


Figure 25. Correlation between measured change in exhaust piston lip temperature and predicted percentage change in hot spot area on the lip for spray angle variation at 70% load.

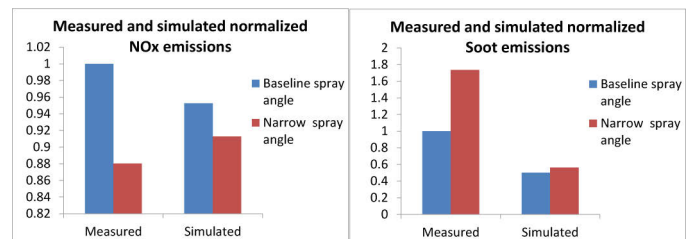


Figure 27. Comparison of trends in the measured and simulated results of normalized NOx and soot emissions for spray angle variation at 70% load conditions.

Consider [Figure 25](#), which compares the measured change in average exhaust piston lip temperature and the predicted percentage change in hot spot areas on the lip for the Baseline and the narrower spray angle cases. Here, the predicted percentage changes in hot spot area are computed over the High and Low temperature bins as discussed before, as well as a single large bin, $0.7T_{max} \leq T_{near\ wall} \leq T_{max}$. A significant reduction ($\sim 41\%$) in the High bin hot spot area is observed with the narrower spray angle injector relative to the Baseline injector. Hence, it is consistently seen with respect to both injector clocking and spray angle variation, trends in the high temperature bin hot spot area correlate with trends in the measured thermocouple temperatures on the bowl lip. It is interesting to observe from [Figure 25](#) that there is about a 20% increase in the hot spot area in the Low bin and an 18% increase over the single large bin with the narrower spray angle injector. As in the case of the clocking study, this further indicates that a configuration that yields favorable piston thermal management (e.g. Clocking 3 and Narrower spray angle) redistributes the near-wall hot gases into a lower temperature zone. Furthermore, the trends observed in [Figure 25](#) underscore the importance of resolving the hot spot area calculation through multiple temperature bins as a single large bin (e.g. $0.7T_{max} \leq T_{near\ wall} \leq T_{max}$) does not capture the trends observed in the piston temperature measurements.

Comparisons of trends in the percentage change in the closed-cycle power (with respect to the Baseline) computed from the measured and simulated results for the two spray angle cases are shown in [Figure 26](#). About 1% penalty in CCP with the narrower spray angle relative to the Baseline spray angle is observed based on the measured data, whereas simulated results indicate about the same CCP for both injectors. However, given measurement uncertainties that could result in an error band of 0.5-1% in CCP, it is reasonable to assume that both measurements and simulations indicate comparable CCP for the two injectors. Trends in normalized NOx and soot emissions are shown in [Figure 27](#). Note that the normalization here is based on the measured NOx and soot emissions for the Baseline spray angle scenario. Good agreement is seen in the trends in both NOx and soot between measured and simulated results, though sensitivities are underestimated in the simulations. For instance, measurements indicate about 12% reduction in NOx with the narrower spray angle, whereas simulated results yield about 4% reduction. In the case of soot emissions, a noticeable increase in the soot level is obtained with the narrower spray injector in the measurements, though both scenarios correspond to relatively low soot levels (< 0.3 g per kg of fuel), while the simulations predict only a small increase. Ongoing CFD studies exploring a wider range of data are more focused on improving both qualitative and quantitative agreement between measured and predicted emissions characteristics.

This section is concluded by investigating the plume/wall interactions at the 70% load condition for the Baseline and narrower spray angle injectors. Consider [Figures 28, 29, 30, 31, 32](#), which show the plume/wall interactions for the Baseline and narrower spray angle injectors at different crank angles. As before, we depict only the exhaust piston for clarity, and plot the stoichiometric isosurfaces along with the piston surface colored by near wall gas temperatures. Notice from [Figure 28](#) that for the narrower spray angle injector, the cone angle of the individual plumes is large enough to cause plume-to-plume interactions, while the Baseline injector plumes penetrate into the chamber distinct from each other. It is understandable that such plume-to-plume interactions reduce oxygen entrainment between plumes and result in greater soot formation. It is interesting to observe from [Figure 29](#) that, in fact, the narrower plumes impinge earlier on the piston lip surface relative to the Baseline injector plumes. This is due to a higher penetration rate which, in turn, results in shallower targeting on the lip surface. The higher penetration arises due to interacting plumes (see [Figure 28](#)) in the case of narrower spray angle injector with higher effective momentum to overcome the swirling effects of the charge motion that act to propel the plumes toward the piston walls. As seen from [Figures 29, 30, 31, 32](#), the Baseline injection plumes impinge deeper and spread significantly on the lip, whereas the narrower spray angle plumes spread predominantly above the lip and detach from the surface as the pistons move apart during the expansion stroke.

effects of injection spray angle on plume/wall interactions and their impact on piston thermal management.

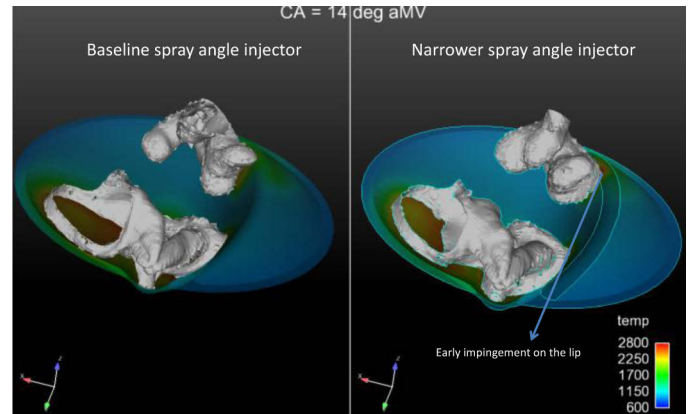


Figure 29. Plume/wall interactions compared between the two injectors at 14 degree aMV crank angle at 70% load conditions.

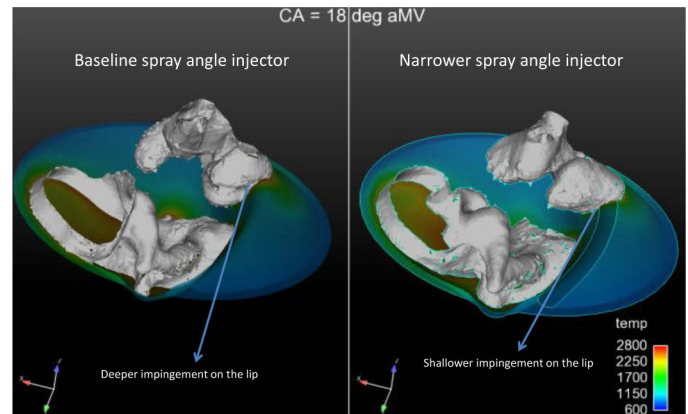


Figure 30. Plume/wall interactions compared between the two injectors at 18 degree aMV crank angle at 70% load conditions

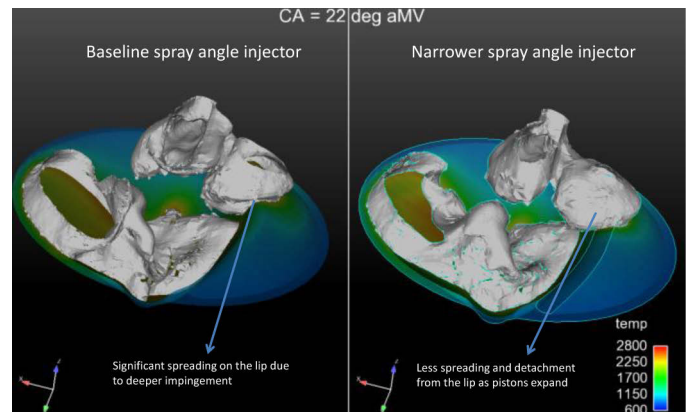


Figure 31. Plume/wall interactions compared between the two injectors at 22 degree aMV crank angle at 70% load conditions.

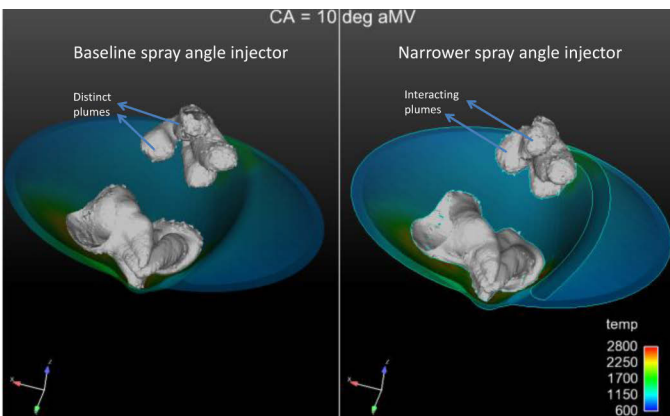


Figure 28. Plume/wall interactions compared between the two injectors at 10 degree aMV crank angle at 70% load conditions.

These visual trends are further confirmed and quantified in [Figures 33 and 34](#), which compare the transient hot spot area on the exhaust piston lip computed over the High and Low temperature bins for the two spray angle cases. In agreement with [Figure 29](#), we see an earlier generation of hot spot area in the High temperature bin for the narrower spray angle injector, but much lower peak area relative to the Baseline injector. Similar trends are seen with respect to the Low bin as well, though a larger average hot spot area is produced by the narrower plumes, as lower temperature gases interact more with the piston lip relative to the Baseline injection plumes. Hence, CFD results provide valuable insight into the

SUMMARY/CONCLUSIONS

In this work, the effects of injection pattern design on piston thermal management in an OP2S engine were investigated through a combined experimental and analytical approach. A proprietary telemetry system was employed to measure temperatures at various locations on the piston surfaces during tests on a single-cylinder 1.6L research engine. Injection pattern was varied through variation of the injector clocking angle and the injection spray angle. Operating conditions at two different indicated power levels (50% and 70% load) were measured to understand the impact of injector clocking and injection spray angle on piston thermal management. A well-correlated, detailed, chemistry-based combustion-CFD model was employed to simulate the measured conditions, and gain insight into mechanisms affecting piston thermal management when the injection pattern is varied.

A novel methodology based on hot spot area calculations was employed as part of this study to correlate measured trends in piston temperatures under different power conditions. It was consistently found that the predicted trends in exhaust piston lip hot spot area in the High temperature bin correlated well with trends in the measured exhaust lip temperatures. With respect to injector clocking variation at the 50% load condition, the favorable clocking arrangement from measurements for lowering piston lip temperatures resulted in a significant reduction in the High bin hot spot area by targeting the injection plumes below the lip surface.

Spray angle variation was studied at the 70% load operating condition through measurements and simulation of injectors with a Baseline and 2.5 degree narrower spray angles. Simulated results showed a significant reduction in the High temperature bin hot spot area with the narrower spray angle injector, which correlated well with lower temperatures measured on the exhaust piston lip relative to the Baseline injector. Detailed flowfield comparisons of the two injectors revealed higher penetration and shallower targeting of the narrower plumes on the lip surface, which lowered the extent of spreading of the plumes on the lip and the resulting hot spot areas as the pistons move apart during the expansion phase. CFD results directionally predicted the measured trends in performance and emissions with spray angle variation. Studies are in progress to better understand and improve combustion model fidelity for both qualitatively and quantitatively predicting tradeoffs between piston thermal management, performance and emissions in opposed-piston engines. The present study unlocks the potential and degree of freedom in the injection pattern design in an OP2S engine to improve piston thermal management while optimizing combustion performance and emissions.

REFERENCES

1. Flint, M. and Pirault, J.P., "Opposed Piston Engines: Evolution, Use, and Future Applications," SAE International,

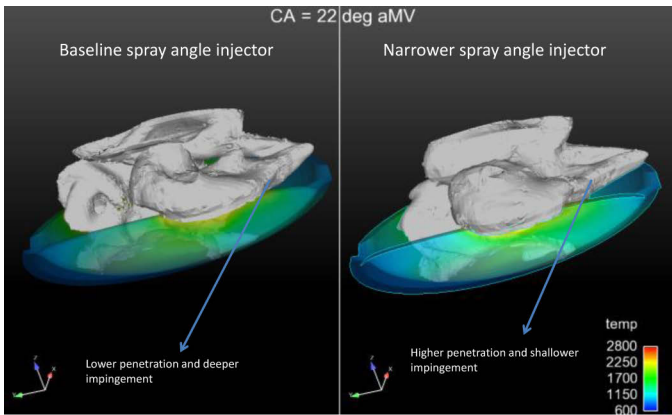


Figure 32. Plume/wall interactions compared between the two injectors at 22 degree aMV crank angle at 70% load conditions (side view to show plume penetration differences).

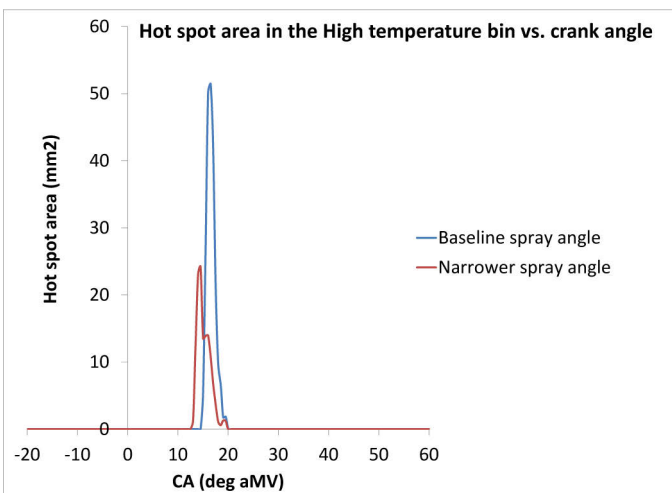


Figure 33. Hot spot area in the High temperature bin as a function of crank angle for the two spray angle cases at 70% load conditions.

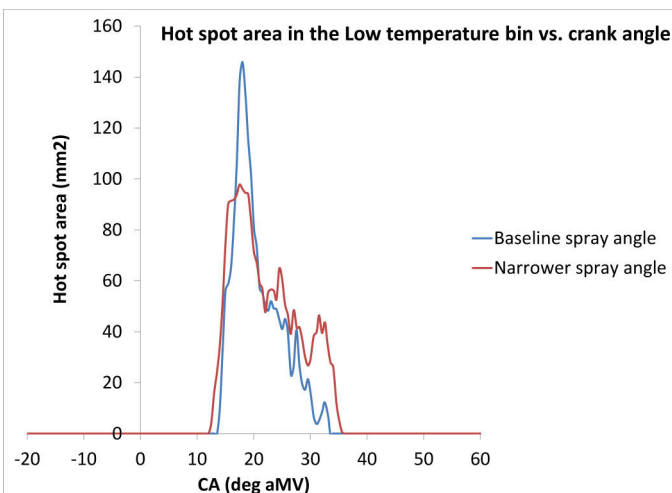


Figure 34. Hot spot area in the Low temperature bin as a function of crank angle for the two spray angle cases at 70% load conditions.

Warrendale, PA, ISBN 978-0-7680-1800-4, 2009, doi:
[10.4271/R-378](https://doi.org/10.4271/R-378).

2. Johnson, D., Wahl, M., Redon, F., Dion, E., McIntyre, S., Regner, G., and Herold, R., "Opposed-Piston Two-Stroke Diesel Engine - A Renaissance," Symposium on International Automotive Technology (SIAT), Jan 2011.

3. Regner, G., Herold, R., Wahl, M., Dion, E. et al., "The Achates Power Opposed-Piston Two-Stroke Engine: Performance and Emissions Results in a Medium-Duty Application," *SAE Int. J. Engines* 4(3):2726-2735, 2011, doi:
[10.4271/2011-01-2221](https://doi.org/10.4271/2011-01-2221).

4. Herold, R., Wahl, M., Regner, G., Lemke, J. et al., "Thermodynamic Benefits of Opposed-Piston Two-Stroke Engines," SAE Technical Paper [2011-01-2216](https://doi.org/10.4271/2011-01-2216), 2011, doi:
[10.4271/2011-01-2216](https://doi.org/10.4271/2011-01-2216).

5. Fuqua, K., Redon, F., Shen, H., Wahl, M., and Lenski, B., "Combustion Chamber Constructions for Opposed-Piston Engines," U.S. Patent Application US20110271932.

6. Regner, G., Koszewnik, J., Redon, F., and Dion, E., "Modernizing the Opposed-Piston, Two-Stroke Diesel Engine for More Efficient Commercial Vehicle Applications," 7th MTZ Conference Heavy-Duty, On- and Off-Highway Engines, Nov. 2012.

7. Lee, P. and Wahl, M., "Cylinder Cooling for Improved Durability on an Opposed-Piston Engine," SAE Technical Paper [2012-01-1215](https://doi.org/10.4271/2012-01-1215), 2012, doi:
[10.4271/2012-01-1215](https://doi.org/10.4271/2012-01-1215).

8. Senecal, P., Richards, K., Pomraning, E., Yang, T. et al., "A New Parallel Cut-Cell Cartesian CFD Code for Rapid Grid Generation Applied to In-Cylinder Diesel Engine Simulations," SAE Technical Paper [2007-01-0159](https://doi.org/10.4271/2007-01-0159), 2007, doi:
[10.4271/2007-01-0159](https://doi.org/10.4271/2007-01-0159).

9. Richards, K.J., Senecal, P.K., Pomraning, E., "CONVERGE (Version 1.4.1)," Convergent Science Inc., Middleton, WI, 2012.

10. Patel, A., Kong, S., and Reitz, R., "Development and Validation of a Reduced Reaction Mechanism for HCCI Engine Simulations," SAE Technical Paper [2004-01-0558](https://doi.org/10.4271/2004-01-0558), 2004, doi:
[10.4271/2004-01-0558](https://doi.org/10.4271/2004-01-0558).

11. Hiroyasu, H. and Kadota, T., "Models for Combustion and Formation of Nitric Oxide and Soot in Direct Injection Diesel Engines," SAE Technical Paper [760129](https://doi.org/10.4271/760129), 1976, doi:
[10.4271/760129](https://doi.org/10.4271/760129).

12. Nagle, J., and Strickland-Constable, R.F., "Oxidation of Carbon Between 1000-2000 C," Proceedings of the Fifth Carbon Conference, Vol. 1, p.154, 1962.

13. Patterson, M.A., "Modeling the Effects of Fuel Injection Characteristics on Diesel Combustion and Emissions," Ph.D. Thesis, University of Wisconsin-Madison, 1997.

14. O'Rourke, P.J., "Collective Drop Effects on Vaporizing Liquid Sprays," Ph.D. Thesis, Princeton University, 1981.

15. Han, Z., and Reitz, R.D., "Turbulence Modeling of Internal Combustion Engines Using RNG k- ϵ Models," *Combustion Science and Technology*, Vol. 106, 1995.

16. Klyza, C., "Optical Measurement Methods used in Calibration and Validation of Modeled Injection Spray Characteristics," Poster P7, presented in the 2010 Directions in Engine-Efficiency and Emissions Research (DEER) Conference.

ACKNOWLEDGMENTS

The authors are very thankful to Nicholas Rakovec of Achates Power, Inc. for the collection and processing of the measured data reported in this study, and Gilbert Kammerer for providing details on the telemetry system employed in the engine experiments. We are also thankful to the Leadership Team at Achates Power for many valuable suggestions and directions on the studies presented in this work.

DEFINITIONS/ABBREVIATIONS

CFD - Computational Fluid Dynamics

EGR - Exhaust Gas Recirculation

FEA - Finite Element Analysis

IFR - Injection Flow and Rate

NO_x - Nitrogen Oxides

OP2S - Opposed-Piston Two-Stroke

RNG - Renormalization Group

ϵ - Turbulent Dissipation Rate

g - Gram

kg - Kilogram

k - Turbulent Kinetic Energy

The Engineering Meetings Board has approved this paper for publication. It has successfully completed SAE's peer review process under the supervision of the session organizer. This process requires a minimum of three (3) reviews by industry experts.

All rights reserved. No part of this publication may be reproduced, stored in a retrieval system, or transmitted, in any form or by any means, electronic, mechanical, photocopying, recording, or otherwise, without the prior written permission of SAE.

ISSN 0148-7191

Positions and opinions advanced in this paper are those of the author(s) and not necessarily those of SAE. The author is solely responsible for the content of the paper.

SAE Customer Service:

Tel: 877-606-7323 (inside USA and Canada)

Tel: 724-776-4970 (outside USA)

Fax: 724-776-0790

Email: CustomerService@sae.org

SAE Web Address: <http://www.sae.org>

Printed in USA